The Astrophysical Journal Letters, 1002:L2 (8pp), 2026 May 1 https://doi.org/10.3847/2041-8213/ae5ca4

Active-region Modulation of Subsurface Meridional Flows and Magnetic Flux Transport on the Sun

Anisha Sen[1,2], S.P. Rajaguru[1,2], Ruizhu Chen[3], Junwei Zhao[3], and Shukur Kholikov[4]
[1] Indian Institute of Astrophysics, II Block, Koramangala, Bengaluru 560 034, India; anisha.sen@iiap.res.in, rajaguru@iiap.res.in
[2] Pondicherry University, R.V.Nagar, Kalapet, Puducherry 605014, India
[3] W. W. Hansen Experimental Physics Laboratory, Stanford University, Stanford, CA 94305-4085, USA
[4] National Solar Observatory, Boulder, CO, USA
Received 2026 February 21; revised 2026 April 6; accepted 2026 April 8; published 2026 April 20

Abstract

Using time–distance helioseismology applied to 14 yr of Solar Dynamics Observatory/Helioseismic and Magnetic Imager observations spanning solar cycle 24 and the rising phase of cycle 25, we present evidence that meridional flows in the lower half of the near-surface shear layer (NSSL), modulated by active-region magnetic fields, play a central role in the episodic global transport of magnetic flux. In particular, polar-field buildup is tightly linked to plasma outflows diverging from active latitudes within the deeper NSSL. The magnitude and timing of hemispheric polar-field evolution are regulated by depth-dependent meridional flow, including its cross-equatorial component, responding to active-region flux asymmetries. During cycle 24 maximum, stronger southern outflows accelerated flux transport, causing the southern polar field to peak nearly 4 yr before the northern. Global magnetic flux transport patterns in the previous three solar cycles (21, 22, and 23) show broad consistency with the deeper meridional flow modulation inferred in cycles 24 and 25. These results identify activity-dependent flow variations in deeper layers of the NSSL as a dynamically significant component of the Babcock–Leighton process that governs the generation and hemispheric asymmetry of the global dipole field.

Unified Astronomy Thesaurus concepts: Solar physics (1476); Helioseismology (709); Solar cycle (1487); Solar meridional circulation (1874); Solar magnetic fields (1503)

1. Introduction

The physical processes that control the transport and redistribution of solar photospheric magnetic field, collectively described as surface flux transport (SFT; A. R. Yeates et al. 2023), form the crucial closing loop producing large-scale poloidal field for the cyclic operation of solar dynamo in a class of models known as the Babcock–Leighton flux transport (BLFT) dynamos (P. Charbonneau 2014). Over the years since its inception (H. W. Babcock 1961; R. B. Leighton 1964, 1969), the BLFT models have been developed, incorporating key observed phenomena behind the near-surface evolution of magnetic fields. A major development has been the inclusion of large-scale meridional circulation in the BLFT models, providing ways to explain several observed features of the solar cycle (Y.-M. Wang & N. R. Sheeley 1991; A. R. Choudhuri et al. 1995). Currently, this area of research has seen intense efforts to develop observational data-driven modeling of the evolution of magnetic fields due to both mean flows and turbulent convection, and their variability linked to the emergence and formation of magnetic structures themselves, and thus acting as a self-regulating feedback loop (R. H. Cameron & M. Schüssler 2010; J. Jiang et al. 2010; R. D. Nandy et al. 2011; R. H. Cameron & M. Schüssler 2012; M. S. Miesch & M. Dikpati 2014; J. Jiang et al. 2015; G. Hazra et al. 2023; K. Teweldebirhan et al. 2024).

Following early observational attempts to measure polar magnetic fields and their cyclic variation (H. W. Babcock & H. D. Babcock 1955; H. D. Babcock 1959; L. Svalgaard et al. 1978), L. Svalgaard et al. (2005) and L. Svalgaard & Y. Kamide (2013) demonstrated that the strength of the polar fields near solar minimum is a reliable precursor for predicting the amplitude of the subsequent solar cycle, highlighting the central role of polar-field buildup in the solar dynamo process. S. Tsuneta et al. (2008) used high-resolution Hinode/Solar Optical Telescope (SOT) spectropolarimetry to show that the Sun's polar regions contain numerous 1 kG unipolar vertical magnetic flux tubes of the same polarity. Analysis of long-term synoptic data by P. Janardhan et al. (2010) revealed a pronounced drop in polar-field strength from the late decline of cycle 22 into cycle 23, tightly correlated with changes in the meridional flow speed (calculated by D. H. Hathaway & L. Rightmire 2010). Modeling studies by J. Jiang et al. (2010) revealed that activity-related converging inflows toward active latitudes can reduce the peak polar field strength by approximately 18%, while L. Upton & D. H. Hathaway (2014) demonstrated that meridional flow variations during cycle 23 led to a 20% reduction in polar-field amplitude in their data-assimilative SFT model. J. Jiang et al. (2011) used an SFT model with reconstructed sunspot emergence records to successfully reproduce polar and open flux back to 1700, confirming the strong correlation between polar field at activity minimum and the strength of the subsequent sunspot cycle. Further theoretical investigations by D. Nandy et al. (2011) and R. H. Cameron & M. Schüssler (2012) showed that localized meridional-flow perturbations impede poleward magnetic flux transport, weakening the polar fields and strength of subsequent solar cycles. Z.-F. Wang et al. (2020)

analyzed how persistent activity complexes during cycle 24 generated a substantial poleward magnetic flux surge, thereby significantly influencing the evolution of the Sun's polar magnetic fields. More recent high-resolution observations by S. Yang et al. (2024) confirm that latitude-dependent variations in poleward flow can create hemispheric asymmetries in the timing of polar-field reversal.

Based on solar-cycle-long observations of meridional and zonal flows in the Sun's near-surface shear layer (NSSL; M. J. Thompson et al. 1996), A. Sen et al. (2025) showed that near-surface inflows toward active latitudes are part of localized circulation cells around active regions, with outflows at depths below $\approx 0.97R_{\odot}$, coinciding with changes in radial gradient of rotation. A follow-up study by A. Sen et al. (2026) demonstrated that the equatorward part of such outflows drives cross-equatorial flows from the more active hemisphere, facilitating flux cancellation near the equator.

In this Letter, we report results from a thorough investigation of the relationships between the surface flux transport from the active latitudes and the outflows originating beneath them in the lower half of the NSSL in cycle 24 and the rising phase of cycle 25. We also examine the synoptic magnetic fields of the previous three cycles (21–23) for deeper flow-driven signatures in surface flux transport, including those in cross-equatorial flux plumes driven by hemispheric asymmetry in active-region magnetic fields. The Letter is structured as follows: Section 2 outlines the data utilized and a description of the analysis technique. Section 3 presents our findings, and Section 4 discusses and concludes, outlining the broader implications of our results.

2. Data and Analysis Procedure

We employ identically processed helioseismic observations obtained from the space-based Helioseismic and Magnetic Imager (HMI: P. H. Scherrer et al. 2012) onboard NASA's Solar Dynamics Observatory (SDO) and from the ground-based Global Oscillation Network Group (GONG). Time–distance helioseismology (T. L. Duvall et al. 1993) is performed with these datasets to infer the meridional flow (S. P. Rajaguru & H. M. Antia 2015) structure and dynamics within the NSSL. The data sources and analysis approach used in this study are the same as those described by A. Sen et al. (2025), to whom we refer the readers for details and for a discussion on the agreement between HMI and GONG measurements. For the analysis and presentation here, we use only the HMI data. The analysis spans a 14 yr period from 2010 May to 2024 April, one year longer into cycle 25 than used in A. Sen et al. (2025). The measurements were processed at a reduced spatial resolution of $0\overset{\circ}{.}36$ per pixel. To mitigate magnetic contamination in the flow estimates (Z.-C. Liang & D.-Y. Chou 2015; R. Chen & J. Zhao 2017), regions with line-of-sight magnetic field strengths exceeding 40 G were masked out in the Dopplergrams prior to analysis. Meridional flows were derived by inverting for the stream function, ensuring compliance with the continuity equation and, consequently, the conservation of mass (S. P. Rajaguru & H. M. Antia 2015).

For studying the connection between flows and the temporal and latitudinal evolution of sunspot distributions, we use data from the Solar Region Summary provided by the National Oceanic and Atmospheric Administration (NOAA). We have also collected synoptic magnetogram data, extending back to three solar cycles, from multiple sources: data from the National Solar Observatory, Kitt Peak, USA (NSO/Kitt Peak)[5] cover Carrington rotations (CR) 1625-2007; this was followed by data from the Vector Spectromagnetograph (VSM) of the NSO/Synoptic Optical Long-term Investigations of the Sun (SOLIS)[6] for CR 2008-2096, and subsequently data from the SDO/HMI[7] for CR 2097-2301. The complete dataset spans the period from 1975 February 19 to 2025 September 9. Data for eight CRs (1640, 1641, 1642, 1643, 1644, 1854, 2015, and 2041) were unavailable and were filled by interpolation for continuity in the analysis.

A known limitation of the above-described synoptic magnetic maps arises near the solar poles due to projection effects. Hence, for more accurate polar-field measurements, we used data from the Wilcox Solar Observatory (WSO),[8] where the polemost aperture measures the line-of-sight field from approximately 55° latitude to the poles. Monthly averaged WSO data from 1976 May 31 to 2025 September 11 were employed, with four missing months (2022 September, 2022 October, 2024 February, and 2025 May) filled by interpolation. For a consistent comparison between the synoptic and WSO polar-field datasets, the common time interval from 1976 May 31 to 2025 September 11 was used.

3. Results

3.1. Outflows beneath Active Regions and Surface Flux Transport

In this section, we investigate how the active-region-driven local circulations within the NSSL modulate the meridional flows and, consequently, the transport and accumulation of magnetic flux toward the poles. In our previous study (A. Sen et al. 2025), we determined the global scale residuals in meridional flow by subtracting its average over a solar cycle (see, for example, H. M. Antia & S. Basu 2022). Here, however, to highlight better the variations due to active-region magnetic fields, we subtract baseline meridional flow of the Sun determined as an average over the solar minimum period (about 2 yr covering 2019 May–2021 April), when there were no active regions (S. S. Mahajan et al. 2023; A. Sen et al. 2026). The top two panels of Figure 1 present the time–latitude profile of cycle-minimum-subtracted variations in meridional flow, δU_{θ}, at depths of $0.99R_{\odot}$ and $0.95R_{\odot}$, covering the period from 2010 October to 2023 October. We use the sign convention of positive values for poleward flows in both hemispheres. Measurement errors in flows are calculated by repeating the seismic inversions 1000 times with travel times randomly perturbed with estimated errors in observed values (A. Sen et al. 2025). While the near-surface flows are measured at 5σ level or above, those in the deeper layers ($0.95R_{\odot}$) can decrease to 3σ levels: the outflow signals on the poleward side of active latitudes (between 20° and 40°) are in the range of 3–12 $\mathrm{m\,s^{-1}}$, with estimated errors ranging from 0.3 to 1.1 $\mathrm{m\,s^{-1}}$ (see Figure 2). The lower two panels of Figure 1 present the longitudinally averaged photospheric radial magnetic field over time and latitude—the magnetic butterfly diagram—for the same period as for the flows, and together they provide a comprehensive view of the evolution of large-scale flow and magnetic patterns across solar cycle 24

[5] https://nispdata.nso.edu/ftp/kpvt/synoptic/mag/
[6] https://solis.nso.edu/0/vsm/crmaps/
[7] http://jsoc.stanford.edu/
[8] http://wso.stanford.edu/Polar.html

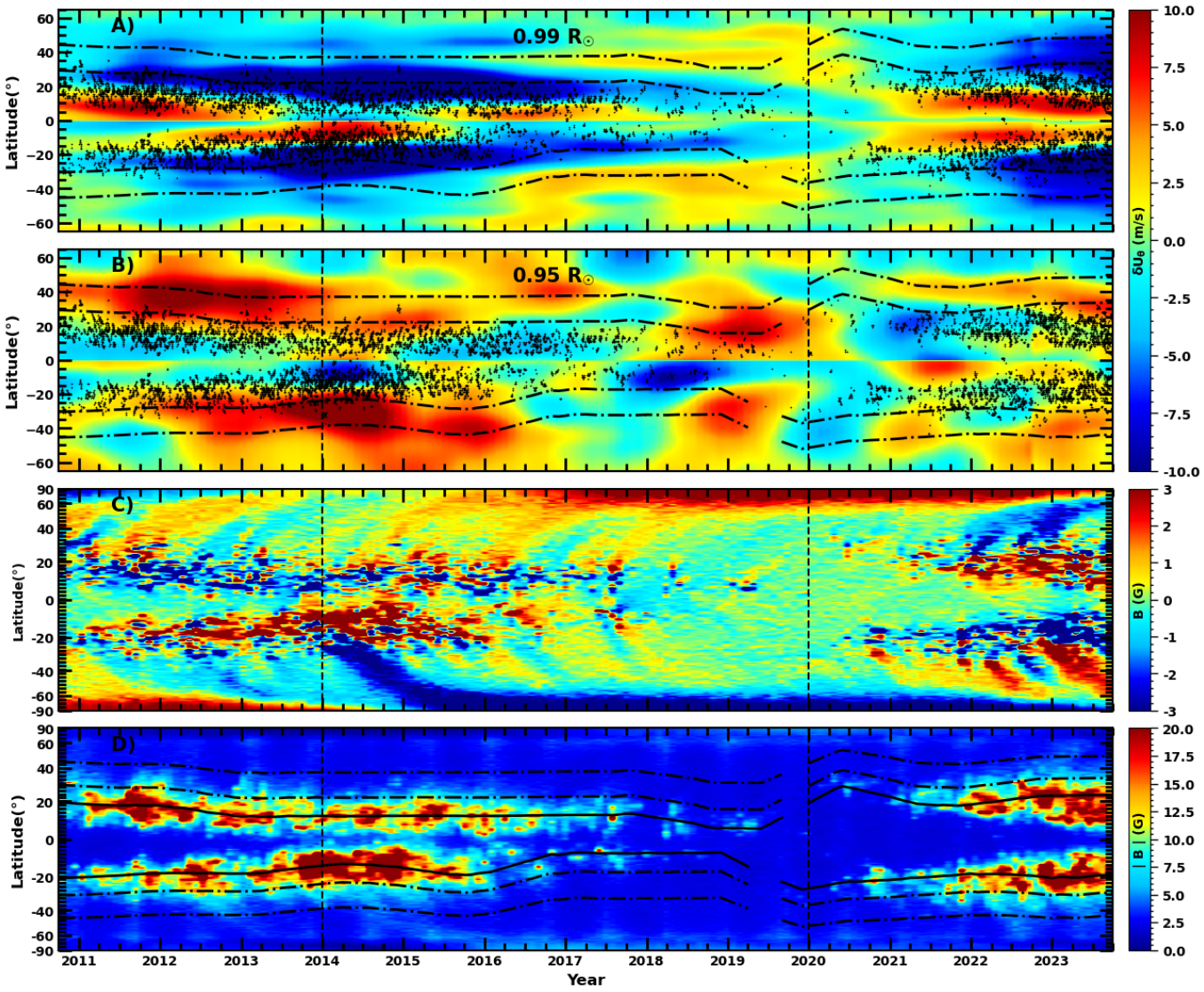

Figure 1. Time–latitude profile of variations in the residual meridional flow at two depths, $0.99R_{\odot}$ and $0.95R_{\odot}$, respectively, are in panels (A) and (B). Positive values correspond to poleward flow in both hemispheres. Corresponding time–latitude variations in the longitudinally averaged signed (i.e., the magnetic butterfly diagram) and unsigned magnetic field are in the lower panels (C) and (D), respectively. The solid line overplotted in panel (D) marks the mean latitude, θ_m, of peak magnetic flux in each hemisphere, and the dotted–dashed lines in panels (A), (B), and (D) enclose the region 10°– 25° away from θ_m. The two vertical dotted lines mark epochs of solar cycle 24 maximum (2014) and minimum (2020). Sunspot locations are overplotted as black dots.

and into the early phase of solar cycle 25: panel (C) shows the signed radial magnetic field, which preserves polarity information and thus allows the tracking of poleward flux transport, polarity reversals, and other large-scale magnetic field evolution processes; panel (D) displays the absolute magnitude of the radial magnetic field, which helps emphasizing the total flux transported as the flow itself does not differentiate the polarity of the fields. Sunspot locations are overplotted as black dots in the panels for the flows.

Comparing meridional flow residuals and the magnetic butterfly diagram in Figure 1, contrary to widely modeled effects of near-surface inflows (J. Jiang et al. 2010; R. H. Cameron & M. Schüssler 2012; L. Upton & D. H. Hathaway 2014), we do not observe any correlation between such flows (top panel of Figure 1) and reduction in poleward transport of magnetic flux. Rather, we observe that the episodic poleward transport of magnetic fields is closely linked with the outflows at the base of the NSSL (depth of $0.95R_{\odot}$, panel (B)): for example, during 2012–2013, the stonger poleward outflow (at $0.95R_{\odot}$) from active latitudes of the northern hemisphere (panel (B)) coincides with enhanced poleward transport of magnetic flux (panel (C)); likewise, during 2014–2016, the strongest poleward flux transport and outflow (at $0.95R_{\odot}$) episodes of cycle 24 coincide in the southern hemisphere.

To examine the above connections more closely, we average the flow residuals δU_{θ} over latitude from 10° to 25° away from the mean latitude, θ_m, of active regions (determined as the latitude of peak flux at each time instant, in each hemisphere) over the northern and southern hemispheres separately. The overplotted solid line in panel (D) of Figure 1 marks θ_m, while the dotted–dashed lines in panels (A), (B), and (D) enclose the region 10°–25° away from θ_m in both hemispheres. The results for flows at the two depths are shown in panels (A) and (B) of Figure 2 (left panel), with solid and dashed lines for northern and southern hemispheres, respectively. Similarly, averaged absolute values of the magnetic field, representing the net flux

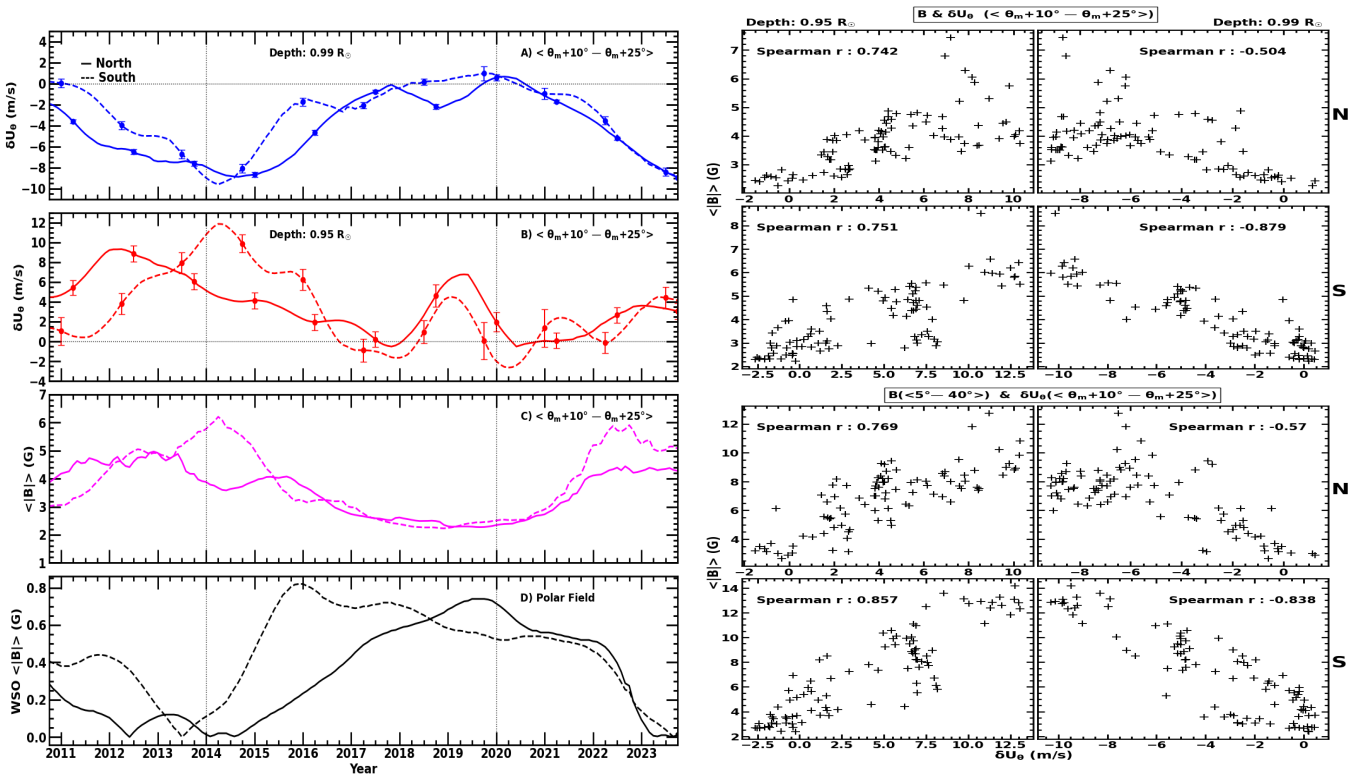

Figure 2. Left: panels (A) and (B) show the residual meridional flows averaged over 10°–25° away from θ_m (marked by dotted–dashed lines in Figure 1) in the northern (solid) and southern (dashed) hemispheres at depths $0.99R_\odot$ and $0.95R_\odot$, respectively. Panel (C) shows the similarly averaged unsigned line of sight (LOS) HMI magnetic field ($|B|$), while panel (D) shows the unsigned polar field from WSO measurements. Right: scatterplots illustrating the correlation between variation of unsigned magnetic field and the flow residuals covering the period of cycle 24 (2010 October–2018 June), along with the estimated Spearman rank correlation coefficients; the top four panels correspond to both quantities averaged over the same latitudinal range (10°–25° away from θ_m), at depths of $0.95R_\odot$ (left column) and $0.99R_\odot$ (right column), for the northern (top row) and southern (bottom row) hemispheres, while the bottom four panels show the correlation between same flow signals against the unsigned magnetic field averaged over the whole active latitude range of 5°–40°.

transported to the poles, are plotted in panel (C). And, we have also used the line-of-sight polar cap magnetic field measurements above 55° latitude from the WSO, and plotted their unsigned amplitudes in panel (D) of Figure 2. We find that during 2014, the flow speed in the southern hemisphere at a depth of $0.95R_\odot$ (red dashed curve in panel (B) of Figure 2) reached its maximum value of about 12 m s^{-1}. This pronounced outflow exhibits a clear association with the magnetic flux over the same latitude range and time plotted as the dashed magenta curve in panel (C) of Figure 2. The resulting poleward transport caused the subsequent accumulation of magnetic flux in the southern pole around 2016, approximately 2 yr later, as shown by the black dashed curve in panel (D) of Figure 2. In contrast, the corresponding poleward accumulation in the northern hemisphere occurred much later, around 2020. The background meridional flow, which is predominantly poleward throughout the NSSL during cycle minima, facilitates the transport of magnetic flux from mid-latitudes toward the poles. During cycle maxima, the outflows beneath active regions, at depths below $0.97R_\odot$, drive the early flux transport toward the poles. Therefore, subsurface outflows are a major driver of the flux transport process: higher flow velocities result in earlier flux arrival at the poles. Our results thus show that the near-surface inflows toward active regions do not significantly alter the flux transport, instead they promote the earlier buildup of polar flux via the deeper outflows to which they connect to.

During cycle 24 minimum (around the year 2020), a clear polar magnetic field asymmetry is observed (Figure 2, panel (D)): the accumulated flux is significantly higher in the northern hemisphere. The early buildup that led to the southern polar field peaking in the year 2016, however, declined in the subsequent years, likely due to the transport of the opposite polarity trailing field of bipolar regions with anti-Hale tilt (A. V. Mordvinov & L. L. Kitchatinov 2019) (or Hale's leading polarity of the hemisphere). In Figure 1 (panel (C)), several surges of leading polarity flux transported toward the pole in the southern hemisphere, during 2016–2019, are seen as due to a relative increase of spot regions that violated the Joy's law (see Figure 1 of A. V. Mordvinov & L. L. Kitchatinov 2019 that identifies anti-Joy and anti-Hale spots from cycle 21–24). These events contributed to the overall weakening of the polar field in the southern hemisphere after 2016. Similarly, a year before the cycle 24 maximum (during 2013), just when the north pole was seeing a reversal with positive polarity flux replacing the previous cycle's negative flux, the active latitudes in the north hosted a few instances of leading polarity negative flux transported toward the pole. This brief burst of negative flux nearly canceled the already reversed pole around 2014, following which a subsequent second reversal happened when normal following polarity flux transport resumed in the north. Therefore, the subsurface outflows beneath active regions, which have surface inflows, drive the flux-transport process regardless of whether the spots are Hale or anti-Hale. Hale spots contribute to building up the polar field, while anti-Hale spots contribute to canceling and thereby weakening the polar flux.

Implicit in our above inferences—that flows at depths below $0.97R_\odot$ advectively transport magnetic flux—is the assumption of high plasma-β conditions, wherein the kinetic energy of flows exceeds the magnetic energy by roughly 1 order of magnitude, at the spatial scales considered. We return to this point in detail in Section 4. We emphasize, however, that our measurements do not directly establish a causal relationship between the flows and flux transport. The inferred flows are from longitudinally averaged travel times and hence cannot be used to track their evolution in and around individual active regions. For the same reasons, our analysis does not allow us to probe the origin or driving mechanisms of these flows.

Despite the above physical considerations, to examine the statistical significance of correlations between flows and magnetic fields, we plot the scatter between them for the active phase of cycle 24 (2010 October–2018 June), with estimates of Spearman rank correlation coefficients, in the right-side panels of Figure 2. The top four panels correspond to both quantities averaged over the same latitudinal range (10°–25° away from θ_m), at depths of $0.95R_\odot$ (left column) and $0.99R_\odot$ (right column), for the northern (top row) and southern (bottom row) hemispheres, while the bottom four panels show the correlation of the same flow signals against the unsigned magnetic field now averaged over the whole active latitude range of 5°–40°. A stronger positive correlation is observed between the magnetic field and the outflow at the deeper layer ($0.95R_\odot$), whereas at $0.99R_\odot$, since the inflows are directed opposite to the flux transport toward higher latitudes, a strong negative correlation between them. Importantly, we find that the correlation coefficient increases when the magnetic field is averaged over the full active latitude range (5°–40°; see the bottom four panels on the right of Figure 2). This signifies that the whole flow system, of course, is due to the active-region magnetic fields themselves, likely due to their interference with the flow of convective energy or thermal causes, although our measurements and correlations studied here cannot address them. The ensuing flows thus draw their energy from the disturbed thermal balance, leading to the dominance of kinetic energy of flows, which then take over the break-up and transport of magnetic flux. We discuss this further in Section 4.

3.2. Subsurface Flow Signatures in the Past Four Solar Cycles

Having identified the roles of active-region-driven meridional flow variations in the magnetic flux transport for cycle 24, we here examine the magnetic butterfly diagrams of the past three cycles—from cycle 21–23—together with cycle 24 and the rising phase of cycle 25. Panel (A) in Figure 3 shows the temporal and latitudinal evolution of the signed magnetic field from cycle 21 to the early phase of cycle 25, derived from NSO Kitt Peak, SOLIS, and HMI synoptic magnetograms. Panel (B) shows the unsigned magnetic fields averaged over latitudes from 10° to 25° away from the mean latitude (θ_m) of active regions in the northern (solid curve) and southern (dashed curve) hemispheres. Drawing parallels with the connections between flows and magnetic flux transport shown in Figure 2, we can identify instances of enhanced flux values with those of outflows in the lower half of the NSSL. Panel (C) shows the unsigned polar fields from the WSO. Comparing panels (B) and (C), we can clearly identify the connections between the north–south asymmetry in subsurface outflow-driven flux transport and that of the polar-field buildup, with a time delay of 2 to 3 yr (see cycles 21, 22, and 24). Cycle 23 polar fields, despite significant asymmetry in active-region flux, had very little asymmetry and were also much weakened, which we identify as due to significant contributions from large non-Hale oriented spots in flux transport across the equator as well as toward the poles.

3.2.1. Cross-equator Flows, Flux Plumes, and Polar Fields

An important consequence of flow circulations flanking the active regions is their cross-equatorial excursions during cycle maxima when spots are relatively closer to the equator with significant hemispheric asymmetry. Such flows transport flux across the equator, leading to cross-equatorial flux plumes. A detailed analysis of such cross-equator flows and flux plumes over cycle 24 was presented in our recent publication (A. Sen et al. 2026). Here, we extend such analysis covering solar cycles 21 to the beginning of cycle 25. Panel (D) of Figure 3 shows the north–south average of signed magnetic field within 5°S–5°N (left y-axis, black), $B_{\rm eq}$, representing the cross-equatorial flux plumes, while the right y-axis has the corresponding hemispheric asymmetry of active-region magnetic field estimated by taking the difference between the absolute magnetic field averaged over active latitudes (5°–40°) in the north and south, $B_{\rm asym} = <|B|_N> - <|B|_S>$. The magnetic N–S asymmetry at active latitudes (red curve) provides a reliable indication of the direction of cross-equatorial flows within the NSSL. For cycle 24, we observed that, during peak activity, most of the flux plumes originated in the magnetically dominant southern hemisphere and migrated toward the northern hemisphere. Interestingly, these plumes moved counter to the direction of near-surface cross-equator flows. This seemingly paradoxical behavior was explained by A. Sen et al. (2026) as due to the return flow (or outflows) at deeper layers (below $0.97R_\odot$), which actually carry magnetic flux across the equator in the reverse direction. The cross-equatorial flux plumes observed across all cycles (bottom panel of Figure 3) show the same connection to north–south magnetic asymmetry at active latitudes (red curve in bottom panel). The flux plumes generally migrate from the more active hemisphere toward the less active one. Because of the sign convention in our definition of the hemispheric magnetic asymmetry ($B_{\rm asym}$), the above-identified correlation between $B_{\rm eq}$ and $B_{\rm asym}$ should alternate between cycles as magnetic polarities reverse from cycle to cycle (Hale's polarity rule): odd cycles would show positive correlation, while the even ones have negative correlation. Panel (D) of Figure 3 largely confirms this connection between $B_{\rm eq}$ and $B_{\rm asym}$, however, with a significant deviation in cycle 23 (during the years mid-2002–2008). We identify this as due to sunspots with non-Hale orientation appearing close to the equator and with significant hemispheric asymmetry. We, in fact, identify a large flux plume of positive polarity that crossed the equator from south to north in 2002 September (see Panel (A) in Figure 3), while the leading polarity in the south, as per Hale's polarity rule, is negative. Since the southern hemisphere was more active during this period, we expect a southward cross-equator flow near the surface with a deeper northward return flow, which actually transports the positive flux of the above-identified non-Hale oriented spot.

In accordance with the expectation that the flux canceled at the equator relates to the global dipole field (R. H. Cameron et al. 2013), we find a strong relationship between the cross-equatorial flux plumes and the evolution of polar-field

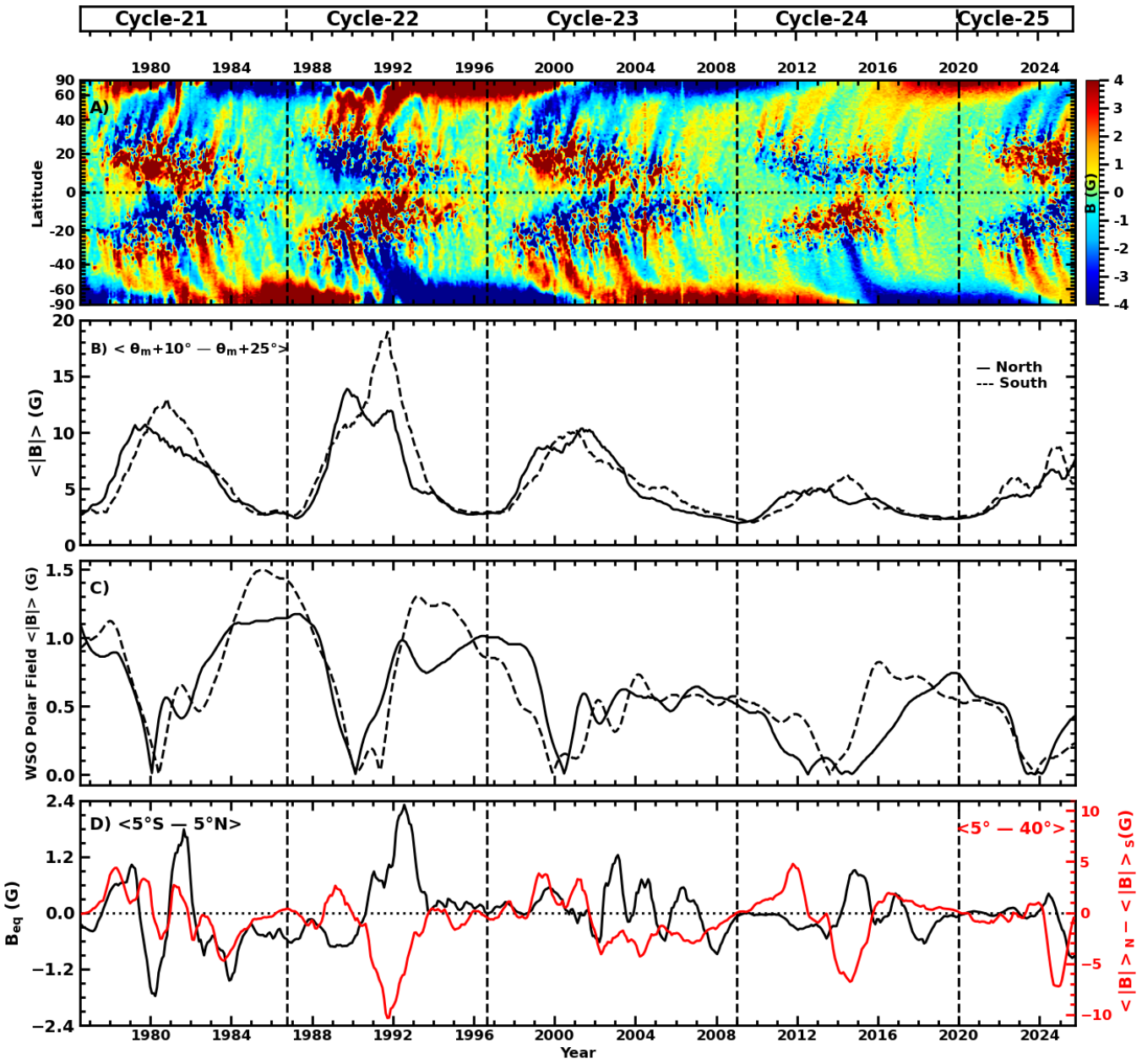

Figure 3. Panel (A) shows the temporal and latitudinal evolution of the longitudinally averaged signed magnetic field from solar cycle 21 to the early phase of cycle 25, based on NSO Kitt Peak, SOLIS, and HMI synoptic magnetograms. Panel (B) shows the unsigned magnetic field ($|B|$) averaged over 10°–25° away from the mean latitude, θ_m, of peak magnetic flux in each hemisphere, while panel (C) shows the unsigned polar field from WSO measurements. In panel (D), the black solid curve is the north–south average of signed magnetic field intensity within 5°S-5°N (left y-axis), $B_{\rm eq}$, that represents the cross-equatorial flux plumes, while the red curve is the hemispheric asymmetry of active-region magnetic field, $B_{\rm asym}$, calculated as the difference between the absolute magnetic field averaged over active latitudes (5°–40°) in the north and south.

asymmetry (panels (C) and (D) of Figure 3). In many instances, the emergence of these plumes appears to modulate the imbalance between the polar fields of the two hemispheres. Typically, the polar field in the hemisphere from which the plume originates strengthens relative to that of the opposite hemisphere. Furthermore, the magnitude of magnetic flux transported across the equator generally correlates well, in magnitude and time, with the enhancement of the polar field in the source hemisphere, which leads to the opposite one in the buildup of polar flux. Although this behavior persists throughout all solar cycles, it becomes particularly evident during the periods around 1984, 1993, and 2015 for cycles 21, 22, and 24: the cross-equatorial flux plumes are of negative, positive and, positive polarity, respectively, and the source hemisphere in all these cases is the southern one with corresponding increases in the southern polar field with very short time lags.

4. Discussion, Conclusions, and Broader Implications

In this work, we have used 14 yr of time–distance helioseismic measurements from SDO/HMI, together with long-term synoptic magnetic field observations spanning four solar cycles, to establish a direct dynamical connection between active-region-driven subsurface flows in the NSSL

and the global transport of magnetic flux that governs polar-field buildup. Our results demonstrate that the episodic poleward and cross-equatorial transport of magnetic flux are primarily regulated by outflows originating beneath active latitudes in the lower half of the NSSL, rather than by near-surface inflows alone (J. Jiang et al. 2010; R. H. Cameron & M. Schüssler 2012; R. H. Cameron et al. 2025).

A central result of this study is that enhanced poleward surges of magnetic flux coincide systematically with strengthened poleward-directed outflows at depths around $0.95R_{\odot}$. These deeper outflows precede the arrival of flux at the poles by one to several years and largely determine the timing and amplitude of polar-field buildup. This behavior is clearly manifested during solar cycle 24, where stronger subsurface outflows in the southern hemisphere during 2013–2015 led to an earlier accumulation of polar flux and a premature southern polar-field maximum around 2016, while the northern hemisphere reached its polar maximum much later, near the cycle minimum in 2020. We have also verified such connections between flows, hemispheric magnetic asymmetry, and polar fields using synoptic magnetograms and WSO measurements covering cycles 21– 25.

Parameterized SFT models showed that converging inflows toward active regions can reduce the effective dipole moment of emerging bipoles and thereby weaken polar fields (J. Jiang et al. 2010), while self-consistent implementations of magnetic-field-dependent inflows demonstrated that such flows provide a nonlinear feedback capable of regulating cycle amplitudes and reproducing the observed correlation between polar fields at solar minimum and the strength of the subsequent cycle (R. H. Cameron & M. Schüssler 2012). At the same time, advection-dominated SFT simulations driven by observed flows established that meridional-flow variations alone cannot explain the weak polar fields preceding cycle 24, highlighting the dominant role of active-region source properties when cycles are intrinsically weak (L. Upton & D. H. Hathaway 2014).

Our helioseismic results provide a critical depth-resolved extension of the SFT framework. By demonstrating that activity-modulated meridional flows are organized as a vertically structured circulation within the NSSL—characterized by near-surface inflows overlying deeper outflows—we provide direct observational support for the physical basis of flow-driven feedback mechanisms inferred in SFT models. Although previous helioseismic studies identified that converging inflows toward active regions near the surface and deeper outflows form circulation cells (D. A. Haber et al. 2002, 2004; B. W. Hindman et al. 2009), our global-scale flow measurements establish the dynamical coupling of deeper outflows and large-scale flux transport. An important physical basis for such deep-layer advection emerging as a dominant mechanism of flux transport derives from the high plasma β conditions at deeper layers, where the deep-rooted flux is more passively advected than at the surface layers. Such a scenerio also emerges from consideration of energetics on the spatial scales that our measurements correspond to: for the Standard Solar Model S (J. Christensen-Dalsgaard et al. 1996), kinetic energy density, $\rho v^2/2$, of typical poleward flows of magnitude of 15 m s^{-1} flanking the active latitudes at depths of $0.95R_{\odot}$, is about 900 J/m^3, which requires field strengths of about 480 G to react back on the flows or to be in equipartition. Since the surface (photospheric) fields are of strength about 10–20 G (see panel (D) Figure 1), intensification of this field by more than a factor of 20, over the depth of 35 Mm, is required for it to reach equipartition, which is highly unrealistic. Three-dimensional MHD simulations of sunspots with 3 kG fields at the photosphere typically achieve stable solutions with about 10–15 kG at depths of 15–20 Mm (M. Rempel 2011), a factor of 4–5 increase in strength. Thus, although the magnetic energy densities at the core regions of active-region flux are in superequipartition to influence the energy transport and thereby cause thermally induced flow systems, the ensuing flows that spread over larger scales hold much larger kinetic energy to advect the disintegrating magnetic flux passively.

Our results are also consistent with, and provide a unifying physical interpretation for, earlier helioseismic and surface-magnetic-field studies that highlighted apparent discrepancies between surface meridional-flow measurements and magnetic flux transport. Using magnetic butterfly diagrams, M. Švanda et al. (2007) showed that the effective poleward flux-transport speed matched better with the mean speed of meridional flows over depths of 3.5–12 Mm inferred from helioseismology, and concluded that the localized flow perturbations around active regions strongly influence longitudinally averaged surface flows, which do not proportionally affect the global transport of magnetic flux. In parallel, J. Zhao et al. (2014) reported an anticorrelation between high-latitude meridional-flow speed and the polarity of poleward-moving magnetic flux during the rising phase of solar cycle 24, suggesting a dynamic coupling between surface flows and polar-field evolution. The depth-resolved and long-term helioseismic measurements presented here reconcile these findings by demonstrating that such surface-level signatures are the manifestation of a vertically structured flow system within the NSSL.

Our analysis further demonstrates that hemispheric asymmetries in polar-field buildup are dynamically regulated by asymmetric subsurface flows, including cross-equatorial components. Periods of strong north–south imbalance in active-region magnetic flux give rise to cross-equatorial outflows in the deeper NSSL, which transport magnetic flux preferentially from the more active hemisphere toward the less active one. Such hemispheric coupling has long been inferred from surface magnetic field evolution (e.g., Y.-M. Wang et al. 2009; J. Jiang et al. 2010), but our results identify a specific subsurface flow mechanism responsible for this coupling and establish its characteristic time delay of approximately 2 to 3 yr.

An important corollary is that the influence of anti-Hale and anti-Joy active regions on polar-field evolution is mediated by the same subsurface flow system. While deeper outflows transport magnetic flux toward the poles largely independent of polarity, the contribution of this flux to the polar field depends sensitively on the polarity orientation and tilt of the emerging regions (e.g., M. Dasi-Espuig et al. 2010; J. Jiang et al. 2014). This explains why strong subsurface outflows do not necessarily lead to sustained polar-field strengthening, as demonstrated by the weakening of the southern polar field after 2016 despite high outflow velocities.

A further important aspect of subsurface outflows identified in this study concerns the production of Joy's law tilt itself, which has recently been attributed to Coriolis force acting on supergranular-scale convective outflows (W. Roland-Batty et al. 2025). The Coriolis force mediation of active-region flows, including its deeper outflows, which operate on larger

spatial and temporal scales, has been well recognized and studied (see A. Sen et al. 2025, and references therein). Hence, although the deeper outflows should contribute to tilt production or modulate the subsequent redistribution of already tilted flux, whether they constitute a subsurface mechanism to generate tilt during the earliest stages of emergence remains an open question requiring high-cadence local helioseismic measurements that image the whole NSSL in latitude and longitude. This aspect relates to the origin of the whole circulatory flow system around active regions: whether they are driven from the surface layers after emergence, or due to processes related to the emerging flux itself as it traverses the deeper layers of the NSSL.

Taken together, these results point to a shallow but dynamically rich nonlinearity in the Babcock–Leighton dynamo, operating predominantly within the NSSL. The NSSL, thus, emerges as the critical interface where surface magnetic activity feeds back onto large-scale flows, which in turn regulate flux transport, hemispheric coupling, and polar-field formation. This perspective reconciles previously divergent interpretations regarding the relative importance of flow variations and active-region source properties by identifying their complementary roles: stochastic variations in flux emergence govern cycle-to-cycle variability, while depth-dependent flow perturbations in the NSSL provide systematic nonlinear regulation (R. H. Cameron & M. Schüssler 2012; L. Upton & D. H. Hathaway 2014).

The broader implication is that solar-cycle predictability is fundamentally controlled by processes occurring in the Sun's outer few percent by radius. The success of polar-field-based predictions, including the correct anticipation of the stronger-than-expected solar cycle 25 (e.g., R. H. Cameron et al. 2016; D. H. Hathaway & L. A. Upton 2016), reflects the limited memory of the solar dynamo and the dominant role of near-surface and subsurface transport processes. Future data-assimilative dynamo and surface flux transport models must therefore incorporate observationally constrained, depth-dependent meridional flows, including their hemispheric and activity-dependent variations, in order to capture the true dynamics of the solar magnetic cycle.

Acknowledgments

The HMI data used are courtesy of NASA/SDO and the HMI science teams. Data preparation and processing have utilized the Data Record Management System (DRMS) software at the Joint Science Operations Center (JSOC) for NASA/SDO at Stanford University. Our sincere thanks go to H.M. Antia for supporting A.S. in performing the inversions. The GONG data used are obtained by the NSO Integrated Synoptic Program, managed by the National Solar Observatory, which is operated by the Association of Universities for Research in Astronomy (AURA), Inc., under a cooperative agreement with the National Science Foundation and with contributions from the National Oceanic and Atmospheric Administration. This work has received funding from the NASA DRIVE Science Center COFFIES Phase II CAN 80NSSC22M0162 to Stanford University. J.Z., R.C., and S.K. were partly sponsored by NASA HGIO grant 80NSSC25K7671. Data-intensive computations in this work have utilized the High-Performance Computing facility at the Indian Institute of Astrophysics. A.S. is supported by INSPIRE Fellowship from the Department of Science and Technology (DST), Government of India. We thank an anonymous referee for valuable suggestions that led to significant improvements and additions to the manuscript.

ORCID iDs

Anisha Sen https://orcid.org/0000-0003-2694-3288
S.P. Rajaguru https://orcid.org/0000-0003-0003-4561
Ruizhu Chen https://orcid.org/0000-0002-2632-130X
Junwei Zhao https://orcid.org/0000-0002-6308-872X
Shukur Kholikov https://orcid.org/0000-0003-1860-3697

References

Antia, H. M., & Basu, S. 2022, ApJ, 924, 19
Babcock, H. D. 1959, ApJ, 130, 364
Babcock, H. W. 1961, ApJ, 133, 572
Babcock, H. W., & Babcock, H. D. 1955, ApJ, 121, 349
Cameron, R. H., Dasi-Espuig, M., Jiang, J., et al. 2013, A&A, 557, A141
Cameron, R. H., Jiang, J., & Schüssler, M. 2016, ApJL, 823, L22
Cameron, R. H., & Schüssler, M. 2010, ApJ, 720, 1030
Cameron, R. H., & Schüssler, M. 2012, A&A, 548, A57
Cameron, R. H., Schunker, H., Brun, A. S., et al. 2025, A&A, 701, A277
Charbonneau, P. 2014, ARA&A, 52, 251
Chen, R., & Zhao, J. 2017, ApJ, 849, 144
Choudhuri, A. R., Schussler, M., & Dikpati, M. 1995, A&A, 303, L29
Christensen-Dalsgaard, J., Dappen, W., Ajukov, S. V., et al. 1996, Sci, 272, 1286
Dasi-Espuig, M., Solanki, S. K., Krivova, N. A., Cameron, R., & Peñuela, T. 2010, A&A, 518, A7
Duvall, T. L., Jr., Jefferies, S. M., Harvey, J. W., & Pomerantz, M. A. 1993, Natur, 362, 430
Haber, D. A., Hindman, B. W., Toomre, J., & Thompson, M. J. 2004, SoPh, 220, 371
Haber, D. A., Hindman, B. W., Toomre, J., et al. 2002, ApJ, 570, 855
Hathaway, D. H., & Rightmire, L. 2010, Sci, 327, 1350
Hathaway, D. H., & Upton, L. A. 2016, JGRA, 121, 10,744
Hazra, G., Nandy, D., Kitchatinov, L., & Choudhuri, A. R. 2023, SSRv, 219, 39
Hindman, B. W., Haber, D. A., & Toomre, J. 2009, ApJ, 698, 1749
Janardhan, P., Bisoi, S. K., & Gosain, S. 2010, SoPh, 267, 267
Jiang, J., Cameron, R. H., Schmitt, D., & Schüssler, M. 2011, A&A, 528, A83
Jiang, J., Cameron, R. H., & Schüssler, M. 2014, ApJ, 791, 5
Jiang, J., Cameron, R. H., & Schüssler, M. 2015, ApJL, 808, L28
Jiang, J., Işik, E., Cameron, R. H., Schmitt, D., & Schüssler, M. 2010, ApJ, 717, 597
Leighton, R. B. 1964, ApJ, 140, 1547
Leighton, R. B. 1969, ApJ, 156, 1
Liang, Z.-C., & Chou, D.-Y. 2015, ApJ, 805, 165
Mahajan, S. S., Sun, X., & Zhao, J. 2023, ApJ, 950, 63
Miesch, M. S., & Dikpati, M. 2014, ApJL, 785, L8
Mordvinov, A. V., & Kitchatinov, L. L. 2019, SoPh, 294, 21
Nandy, D., Muñoz-Jaramillo, A., & Martens, P. C. H. 2011, Natur, 471, 80
Rajaguru, S. P., & Antia, H. M. 2015, ApJ, 813, 114
Rempel, M. 2011, ApJ, 740, 15
Roland-Batty, W., Schunker, H., Cameron, R. H., et al. 2025, A&A, 700, A28
Scherrer, P. H., Schou, J., Bush, R. I., et al. 2012, SoPh, 275, 207
Sen, A., Rajaguru, S. P., Chen, R., Zhao, J., & Kholikov, S. 2026, ApJ, 997, 57
Sen, A., Rajaguru, S. P., Iyer, A. G., et al. 2025, ApJL, 984, L1
Svalgaard, L., Cliver, E. W., & Kamide, Y. 2005, GeoRL, 32, L01104
Svalgaard, L., Duvall, T. L., Jr., & Scherrer, P. H., Jr. 1978, SoPh, 58, 225
Svalgaard, L., & Kamide, Y. 2013, ApJ, 763, 23
Švanda, M., Kosovichev, A. G., & Zhao, J. 2007, ApJL, 670, L69
Teweldebirhan, K., Miesch, M., & Gibson, S. 2024, SoPh, 299, 42
Tsuneta, S., Ichimoto, K., Katsukawa, Y., et al. 2008, ApJ, 688, 1374
Thompson, M. J., Toomre, J., Anderson, E. R., et al. 1996, Sci, 272, 1300
Upton, L., & Hathaway, D. H. 2014, ApJ, 780, 5
Wang, Y.-M., Robbrecht, E., & Sheeley, N. R., Jr. 2009, ApJ, 707, 1372
Wang, Y.-M., & Sheeley, N. R., Jr 1991, ApJ, 375, 761
Wang, Z.-F., Jiang, J., Zhang, J., & Wang, J.-X. 2020, ApJ, 904, 62
Yang, S., Jiang, J., Wang, Z., et al. 2024, RAA, 24, 075015
Yeates, A. R., Cheung, M. C. M., Jiang, J., Petrovay, K., & Wang, Y.-M. 2023, SSRv, 219, 31
Zhao, J., Kosovichev, A. G., & Bogart, R. S. 2014, ApJL, 789, L7